

RESEARCH ARTICLE

10.1002/2017JA025121

Large-Scale Survey of the Structure of the Dayside Magnetopause by MMS

Key Points:

- The paper concerns generation and initial utilization of a database for 8,670 magnetopause and magnetosheath current sheet crossings by MMS1
- We provide the statistics for the duration, motion, and thicknesses of the magnetopause current sheet
- We apply the Walén relation to find crossings that are rotational discontinuities and thus may indicate ongoing magnetic reconnection

Correspondence to:

G. Paschmann,
goetz.paschmann@mpe.mpg.de

Citation:

Paschmann, G., Haaland, S. E., Phan, T. D., Sonnerup, B. U. Ö., Burch, J. L., Torbert, R. B., et al. (2018). Large-scale survey of the structure of the dayside magnetopause by MMS. *Journal of Geophysical Research: Space Physics*, 123, 2018–2033. <https://doi.org/10.1002/2017JA025121>

Received 11 DEC 2017

Accepted 9 FEB 2018

Accepted article online 15 FEB 2018

Published online 30 MAR 2018

G. Paschmann¹ , S. E. Haaland^{2,3} , T. D. Phan⁴ , B. U. Ö. Sonnerup⁵ , J. L. Burch⁶ , R. B. Torbert⁷ , D. J. Gershman^{8,9} , J. C. Dorelli⁸ , B. L. Giles⁸ , C. Pollock¹⁰ , Y. Saito¹¹ , B. Lavraud¹² , C. T. Russell¹³ , R. J. Strangeway¹³ , W. Baumjohann¹⁴ , and S. A. Fuselier^{6,15} 

¹Max-Planck-Institut für extraterrestrische Physik, Garching, Germany, ²Birkeland Centre for Space Science, University of Bergen, Bergen, Norway, ³Max-Planck-Institut für Sonnensystemforschung, Göttingen, Germany, ⁴Space Sciences Laboratory, University of California, Berkeley, Berkeley, CA, USA, ⁵Thayer School of Engineering, Dartmouth College, Hanover, NH, USA, ⁶Southwest Research Institute, San Antonio, TX, USA, ⁷Space Science Center, University of New Hampshire, Durham, NH, USA, ⁸NASA Goddard Space Flight Center, Greenbelt, MD, USA, ⁹Department of Astronomy, University of Maryland, College Park, MD, USA, ¹⁰Denali Scientific, Healy, AK, USA, ¹¹Institute for Space and Astronautical Sciences, Sagami-hara, Japan, ¹²Institut de Recherche en Astrophysique et Planétologie, Université de Toulouse, CNRS, CNES, Toulouse, France, ¹³Earth, Planetary, and Space Sciences, University of California, Los Angeles, CA, USA, ¹⁴Space Research Institute, Austrian Academy of Sciences, Graz, Austria, ¹⁵Department of Physics and Astronomy, The University of Texas at San Antonio, San Antonio, TX, USA

Abstract This paper describes the generation and initial utilization of a database containing 80 vector and scalar quantities, for a total of 8,670 magnetopause and magnetosheath current sheet crossings by MMS1, using plasma and magnetic field data from the Fast Plasma Investigation, Fluxgate Magnetometer, and Hot Plasma Composition Analyzer instruments, augmented by solar wind and interplanetary magnetic field data from CDAWeb. Based on a determination of the current sheet width, measured and calculated vector and scalar quantities are stored for the two sides of the current sheet and for selected times within the current sheet. The only manual operations were the classification of the current sheets according to the type of boundary, the character of the magnetic field transition, and the quality of the current sheet fit. To characterize the database, histograms of selected key quantities are presented. We then give the statistics for the duration, motion, and thicknesses of the magnetopause current sheet, using single-spacecraft techniques for the determination of the normal velocities, obtaining median results of 12.9 s, 38.5 km/s, and 705.4 km, respectively. When scaled to the ion inertial length, the median thickness became 12.6; there were no thicknesses less than one. Next, we apply the Walén relation to find crossings that are rotational discontinuities and thus may indicate ongoing magnetic reconnection. For crossings where the velocities in the outflow region exceed the velocity on the magnetosheath side by at least 250 km/s, 47% meet our rotational discontinuity criteria. If we require the outflow to exceed 250 km/s along the L direction, then the percentage rises to 68%.

1. Introduction

The magnetopause is the boundary that, to first order, shields the Earth's magnetosphere from the shocked solar wind and its embedded interplanetary magnetic field. However, when magnetic reconnection occurs, the magnetosphere and solar wind become magnetically connected so that mass, momentum, and energy can be exchanged. The magnetopause consists of an electric current sheet that achieves the change in orientation and magnitude between the interplanetary magnetic field and Earth's magnetic field. The magnetopause has been studied in situ for a long time, so we have excellent knowledge on its location and shape. But there are only a few extensive studies of its motion, thickness, and internal structure, as well as of in situ studies of the occurrence frequency of the signatures of magnetic reconnection. The Magnetospheric Multiscale Mission (MMS), while primarily targeted at the search for the electron diffusion region, where magnetic reconnection is expected to be initiated, also offers a comprehensive coverage of the dayside magnetopause. A unique feature of the MMS mission is the provision of large numbers of current sheet crossings selected for transmission in burst-mode telemetry via the "Scientist-in-the-Loop" process (e.g., Fuselier et al., 2016),

the result being more than a thousand well-defined magnetopauses. This fact allows us to study the nature of the magnetopause and its current sheet with unprecedented time resolution, both statistically, as well as individually, without users having to first search for and identify the current sheet crossings.

To help exploiting the MMS data, we have built a database, using data from the Fluxgate Magnetometer (FGM) (Russell et al., 2016), the Fast Plasma Investigation (FPI) (Pollock et al., 2016), and the Hot Plasma Composition Analyzer (HPCA) (Young et al., 2016). In the present version we have only included data from MMS 1 spacecraft in the database, but it could easily be expanded to the other MMS spacecraft.

The identification of the current sheet widths is the starting point for building the database. The retrieval of the data from the MMS Science Data Center, their ingestion into the QSAS Science Analysis Software (Allen, 2010), the running of an extensive set of analyses, and the storing of the results in tables in a relational database, is fully automatic. The use of this database enables the use of standardized statements (SQL = Structured Query Language) to assemble statistics on, for example, current sheet thicknesses or the occurrence of signatures of magnetic reconnection based on large numbers of crossings, or to query for crossings with certain specific properties, such as small or large thicknesses, large peak outflow velocities, or current densities, good de Hoffmann-Teller frames, strong heating, deep minima in magnetic field strength, large minor ion densities, large or small upstream plasma β or Mach number, or for any combination of the stored or calculable quantities. These cases can then be analyzed further, for example, employing the four-spacecraft tools available to MMS.

After describing the construction and content of the database in section 2, we present the ranges and averages of parameters that characterize the database in section 3. We then focus on two results: First, the magnetopause duration, motion, and thickness statistics in section 4, and second, the occurrence of rotational discontinuities as indicators of magnetic reconnection in section 5. A summary and conclusions are given in section 6.

2. Data and Methodology

The first step was to download the MMS1 data for mission phases 1a and 1b, (20150901–20170209) from the MMS Science Data center, amounting to a total of 8,670 burst-mode intervals. In the following sections we describe the identification of the current sheets, the analysis steps performed, and what kind of quantities are stored in the database. Technical details, such as the ingestion of the data into the analysis system, the classification of the events, as well as the database accessibility, are described in the Appendix.

2.1. Current Sheet Identification

An important analysis step is the automatic identification of current sheets. This step is based on the maximum variance component, B_L , of the magnetic field, obtained by running standard minimum variance analysis (MVA) on the full burst-mode interval, t_{brst} . The adopted procedure is illustrated by Figure 1, which shows an example of the plots that are generated for all events.

The top panel shows the B_L component during an inbound magnetopause crossing, smoothed for the analysis by a 5 s running average. The search routine finds the midpoint of the B_L transition, from (half) the difference between the maximum and minimum values (the orange line). It then follows the B_L curve until it finds the points that are 38% above and below the 50% level, respectively. These are the dashed red lines, at 12% and 88% of the transition, respectively. The 76% interval between them is taken as the current sheet duration, t_{cs} , as one would if the transition were a Harris current sheet, with a \tanh profile (Harris, 1962). Extending the t_{cs} interval by 50% on both sides, we get the times of the green vertical lines. The 50% extension turned out to cover the full B_L transition in almost all cases. We store the data at the times of the green lines in the database, and use the interval between them for subsequent analyses, such as determination of the Hoffmann-Teller frame and, therefore, refer to it as t_{ht} .

As can be seen from Figure 1, the procedure works very well if the B_L transition is smooth. If there is more than one current sheet in the burst interval, as shown in Figure A1, the procedure picks the one with the largest B_L . More complicated profiles can mislead the search routine but are spotted by the event classification process described in Appendix A2. The latter process also excludes current sheet crossings that are broken up into several contiguous burst segments because so far we have not concatenated adjacent intervals.

In addition to the times based on B_L , the search routine also identifies a number of characteristic times that are based on the plasma data:

Plot layout rev. 21 Aug 2017 (DS revised, GSE coords)

20151206_232844

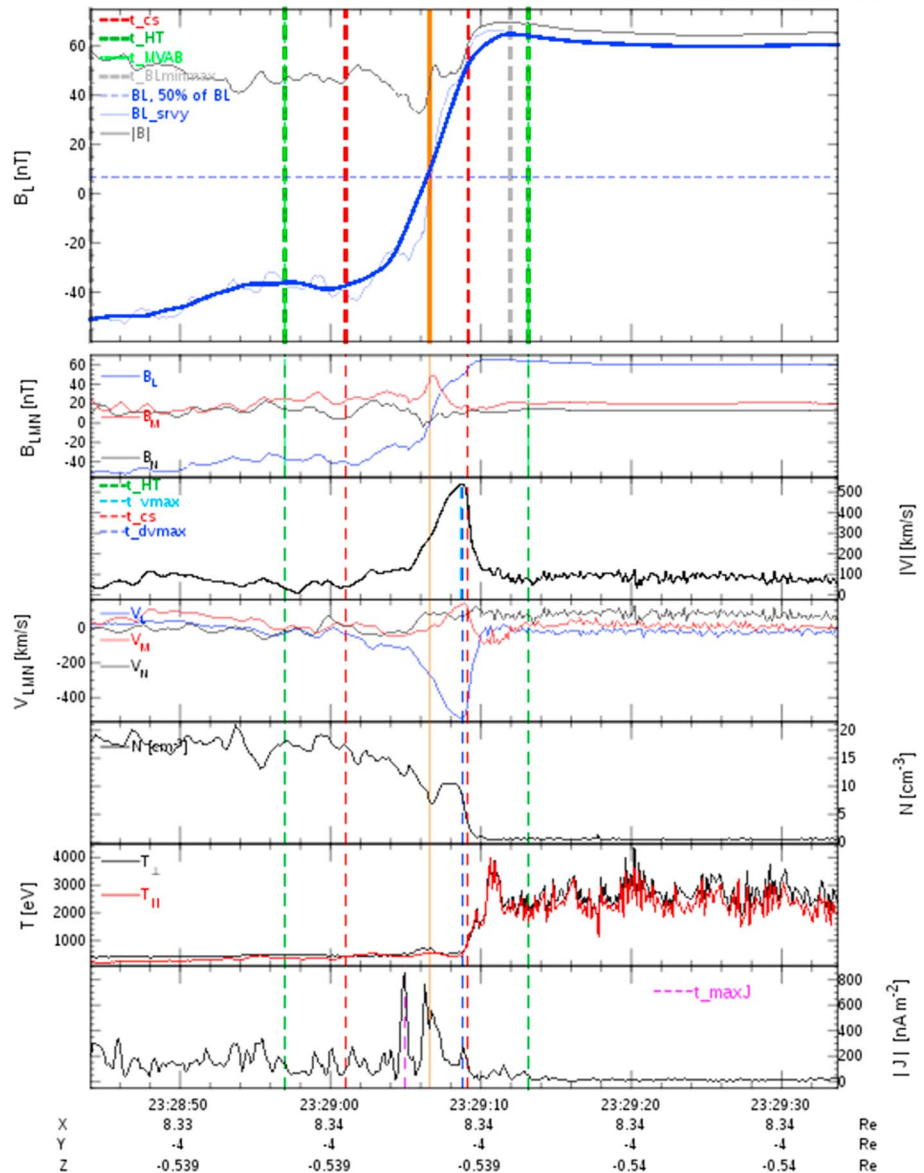


Figure 1. Examples of the plots used to classify MMS current sheet crossings. The top panel shows the B_L component of the magnetic field (full resolution as a thin, smoothed as a thick blue line), and the field magnitude as a thin black line, followed by a panel with all three components of \mathbf{B} , in LMN coordinates; the next four panels show the magnitude and components of the ion bulk velocity, \mathbf{V} , the ion density, N , and parallel (red) and perpendicular (black) temperatures; the bottom panel is the magnitude of the current density, J . The orange vertical line in the top panel marks the center of the current sheet, while the dashed vertical lines on either side mark its width, t_{CS} . The two green lines mark the interval, t_{ht} , twice as long as t_{CS} , used for some analyses and data extraction; blue lines in the lower part mark the times where the magnitudes of \mathbf{V} and $\Delta\mathbf{V}$ maximize, and a purple line the time where the magnitude of J_p maximizes. Characteristic properties of this crossing are as follows: $t_{CS} = 7.9$ s, $V_{max} = 538.7$ km/s, $J_{max} = 854.9$ nA.

1. The time, t_{maxJ} , where the current density J , calculated from the ion and electron bulk velocities and the ion density, maximizes.
2. The time, $t_{max\Delta V}$, where the magnitude of the difference, $\Delta\mathbf{V}$, between the local ion bulk velocity vector and the velocity at the magnetosheath reference time (i.e., at the magnetosheath end of the t_{ht} interval), maximizes.
3. The time where the ion bulk velocity magnitude, V , maximizes.
4. The times where B has a minimum.

The searches for the times in items 1 to 3 are restricted to the interval t_{ht} marked by the green lines in Figure 1, except that the maximum in V is recorded for the full burst-mode event as well. By contrast, the search for the minimum in B is restricted to the current sheet, that is, the interval t_{cs} . We store those times and the respective values of J_p , V , and B in the database. Given the short duration of many of the crossings and their substructures, identification of these characteristic times is possible only because of the unprecedented time resolution of the plasma moments on MMS (150 ms and 30 ms for the ion and electron moments, respectively). The example in Figure 1 has a current sheet that is 7.9 s wide, but the high-speed flow is only 3 s wide, and the current peak only a fraction of a second.

2.2. Data Analysis and Storage

Based on the characteristic times just described, a number of analyses are performed:

1. Run minimum variance analysis (MVA) twice, once in its standard unconstrained version and once in a version where B_n averaged over the analysis interval is constrained to zero (see details in Sonnerup & Scheible, 1998). Store the resulting eigenvalues and eigenvectors for both versions in the database. The analyses under this and the next two items use t_{ht} as the time interval.
2. Run minimum Faraday residue analysis (MFR; see Khrabrov & Sonnerup, 1998; Terasawa et al., 1996) and store the resulting eigenvectors and eigenvalues.
3. Run de Hoffmann-Teller (HT) and Walén analyses (see, e.g., Paschmann & Sonnerup, 2008) and store the HT velocity, V_{HT} , and its correlation coefficient, HT_{cc} , the slope, W_{slope} , and correlation coefficient, W_{cc} , of the Walén analysis.
4. Average the current density J and temperatures $T_{||}$, T_{\perp} over t_{cs} and store these quantities.
5. Extract and store the vectors B , V , and the scalars N , $T_{||}$, T_{\perp} at both ends of the full t_{brst} interval, at both ends of the t_{ht} interval, at $t_{max\Delta V}$, and at t_{maxJ} ; the current density vector J is only stored at t_{maxJ} .
6. Store the H^+ , He^+ , He^{++} , and O^+ densities from the HPCA instrument (Young et al., 2016) at both ends of the t_{ht} interval.
7. Extract and store the interplanetary magnetic field (IMF) and solar wind properties, based on the 1 min OMNI data (King & Papitashvili, 2005) propagated to the magnetopause, at the times close to the beginning and end of the full burst interval.

Note that all vector quantities are stored in GSE coordinates but can be rotated into any of the three coordinate systems by the user, namely, the constrained and unconstrained MVA eigenvector system and also the MFR system, because the corresponding eigenvectors are stored in the database. Derived quantities are not stored but can be readily calculated from the data in the database. Among these are the Alfvén velocity (with and without correction for pressure anisotropies), the plasma β , ion inertial lengths and gyro radii, pressures, and minor ion density ratios. These quantities can be calculated at the two ends of the t_{ht} interval, as well as at the time $t_{max\Delta V}$. Functions that facilitate these calculations have been generated.

2.3. Dayside Magnetopause Current Sheets

The automated procedure described above will pick up any current sheet, including the ones in the magnetosheath, and in the solar wind. Since our focus is on the magnetopause, we first distinguish inbound or outbound crossings. The example in Figure 1 is an inbound magnetopause crossing, as can be seen from the larger B_L on the right. The opposite holds for outbound crossings. Having automatically determined the sense of the crossings, we know which side of the current sheet would be the magnetosheath and which side the magnetosphere. Requiring that $B_L > 20$ nT on the magnetospheric side, we obtain magnetopause crossing candidates. We then further restrict the selection by requiring a magnetic shear $> 45^\circ$, and locations having $|Y| < 10 R_E$. Visual inspection, as described in Appendix A2 then allows us to definitively identify the crossing type and its characteristics.

3. Database Characterization

In the following, a number of properties are presented that characterize the database and illustrate its capabilities, together with some selected results.

3.1. IMF and Solar Wind

The IMF and solar wind plasma conditions propagated to the magnetopause for the times of the crossings in the data base. Figure 2a displays a histogram of the IMF clock angles. There is a predominance of large clock angles because crossings with large magnetic shear usually fit within a single burst interval, while low-shear

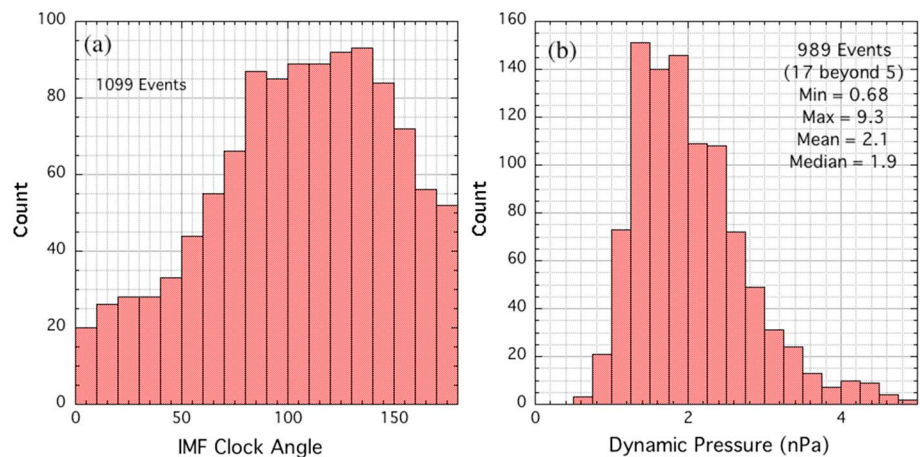


Figure 2. (a) Interplanetary magnetic field clock angles for the 1,099 burst-mode events where interplanetary magnetic field data were available, with 0° and 180° for northward and southward pointing fields, respectively; (b) solar wind dynamic pressures for the 989 magnetopause crossings when solar wind data were available. Minimum, maximum, mean, and medians are given in the insert.

crossings often do not. Figure 2b shows the solar wind dynamic pressure. Its median of 1.9 nPa indicates average conditions.

3.2. Magnetic Shear and Plasma β

Conditions at the magnetopause are presented in Figure 3; Figure 3a shows a histogram of the plasma β upstream of the magnetopause, defined as the ratio of the plasma and magnetic field pressures. The magnetic shear angles across the magnetopause, shown in Figure 3b, exhibit a predominance of large angles, reflecting the bias of the crossing selection, as already mentioned above. The angle scale starts at 45°, because that was the minimum shear we required.

3.3. Magnetopause Structure

A useful characteristic of the database is the maximum ion bulk velocity jumps, which indicate plasma jetting, presumably caused by magnetic reconnection. Figure 4a shows the distribution of maximum velocity jumps, reaching values above 600 km/s. The database also stores the maximum velocities occurring outside the interval t_{ht} , which might indicate the presence of processes other than reconnection.

Figure 4b shows the distribution of maximum current densities, obtained by calculating $J = Nq_e(\mathbf{V}_i - \mathbf{V}_e)$. As the figure shows, there are substantial numbers of crossings with peak current densities exceeding 1,000 nA/m². Large peak current densities are considered candidates of electron diffusion region crossings (e.g., Burch et al., 2016).

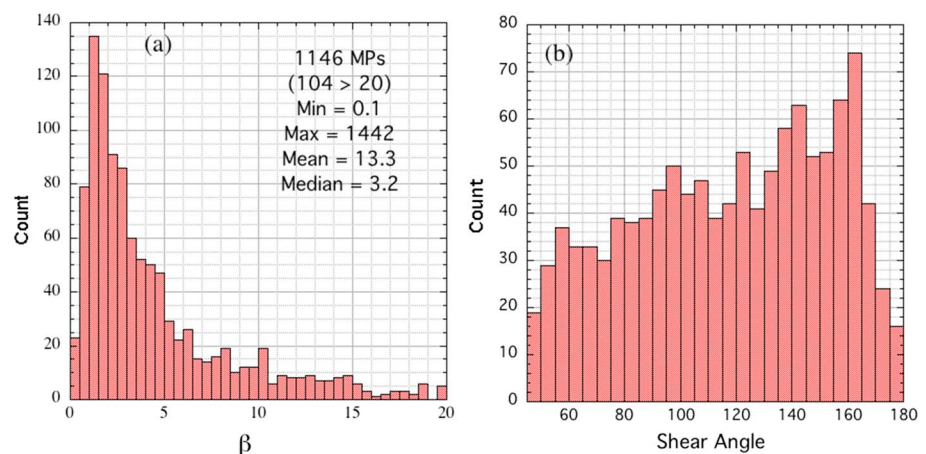


Figure 3. (a) Upstream plasma β ; (b) shear angles across the magnetopause.

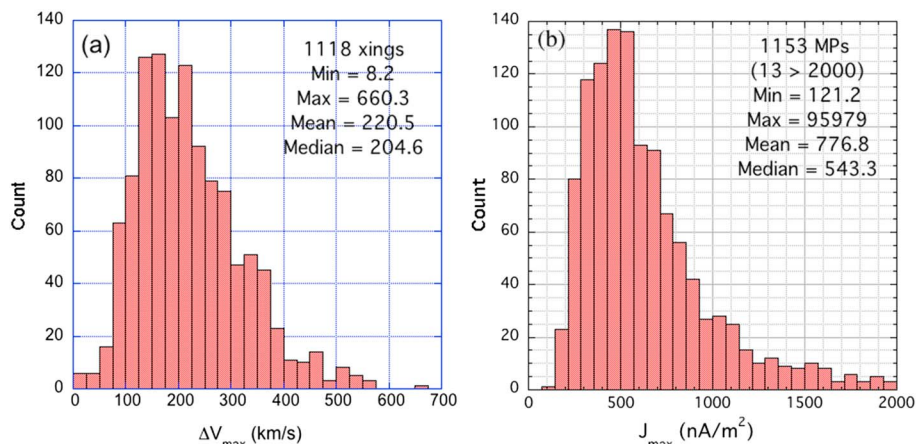


Figure 4. (a) Maximum velocity jumps; (b) maximum current densities.

A frequent feature of the magnetopause is the occurrence of minima in magnetic field strength within the current layer. Figure 5a shows the distribution of events as a function of the ratio between the minimum B within the current sheet and the upstream B . Note that there are more than 100 crossings where B drops to less than 10% of the upstream B . Deep minima in B may be indicative of slow shocks near the switch-off condition (e.g., Sonnerup et al., 2016). Ratios >1 can occur because the search for the minimum B is restricted to the current sheet (interval t_{cs}), while the magnetosheath B is taken at the corresponding end of the t_{ht} interval.

3.4. Ion Composition

The database includes the densities of H^+ , He^+ , He^{++} , and O^+ ions on both sides of the current layer. They help to characterize the plasma environment. As an example we show in Figure 5b the He^{++} percentage measured upstream of the magnetopause, which has a wide range, but a mean that is close to the reported average (3.7%). Querying the database for very high or very low minor ion densities can reveal crossings with unique properties.

4. Magnetopause Duration, Motion, and Thickness

Since the determination of the current sheet duration was the starting point for the construction of the database, we first present the statistics of the duration, motion, and thickness of the magnetopause.

4.1. Duration

For the current sheet duration we take our automatically determined time interval t_{cs} , defined in Figure 1. Its distribution for the 687 magnetopause crossings that satisfied the most stringent conditions, that is, B_L

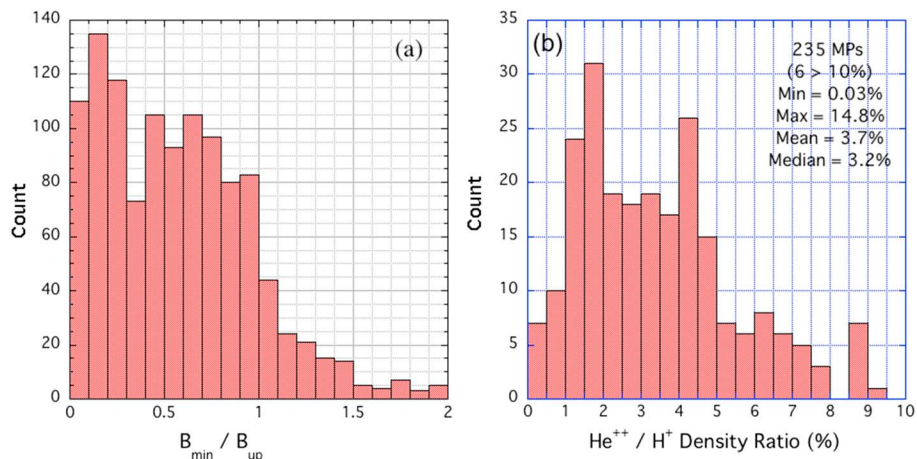


Figure 5. (a) Minimum B within the time interval t_{ht} , scaled to the upstream B ; (b) histogram of the He^{++}/H^+ percentage on the magnetosheath side of the magnetopause.

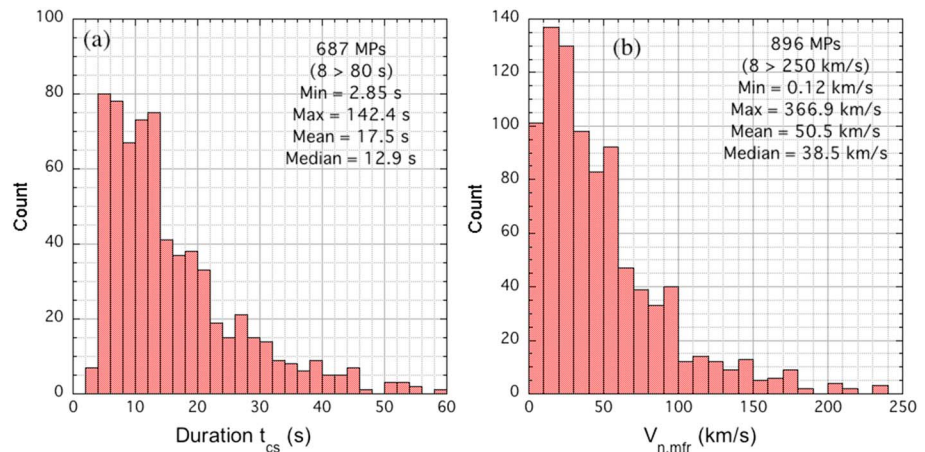


Figure 6. Histograms for the (a) agnetopause crossing durations, t_{cs} , and (b) speed, V_N from Minimum Faraday Residue analysis (MFR). The number of crossings and the minimum, maximum, mean, and median values of t_{cs} are given in the inserts. The numbers of events in the two histograms are different, because the requirements for good t_{cs} are more stringent than those for good V_n from MFR.

profiles classified as “monotonic” and “good fit” (see Appendix A2), is shown in Figure 6a. The predominance of durations between 4 s and 14 s shows that earlier missions would not have resolved such current sheets in their plasma moments, which were obtained every 3 or 4 s.

4.2. Motion

For the normal speeds we have two options, both single-spacecraft methods: either $V_{n,HT}$, the de Hoffmann-Teller velocity dotted into the normal direction from constrained MVA, or $V_{n,MFR}$, the normal speed that results from Minimum Faraday Residue analysis (MFR) (Khrabrov & Sonnerup, 1998; Terasawa et al., 1996). MFR is based on the fact that in a frame moving with a one-dimensional current layer of time-invariant structure, Faraday’s law requires the two components of the electric field tangential to the layer to be constant throughout the layer. To run MFR, we have used the convection electric field, $\mathbf{E} = -(\mathbf{V} \times \mathbf{B})$. Figure 6b shows a histogram of V_n from MFR, for the 896 crossings where the crucial eigenvalue ratio of the MFR was greater than 3. There are more events in the velocity histogram than in the duration histogram, because monotonic B_l profiles and a good fit were not required for the velocities. It will be interesting to compare these single-spacecraft results with MMS four-spacecraft timing, as was achieved already for the Cluster mission (e.g., Haaland et al., 2004).

The two velocities, $V_{n,HT}$ and $V_{n,MFR}$ differ in magnitude and sometimes also in sign. Taking only crossings where the two have the same sign and agree in magnitude to within 50%, we are left with 401 crossings.

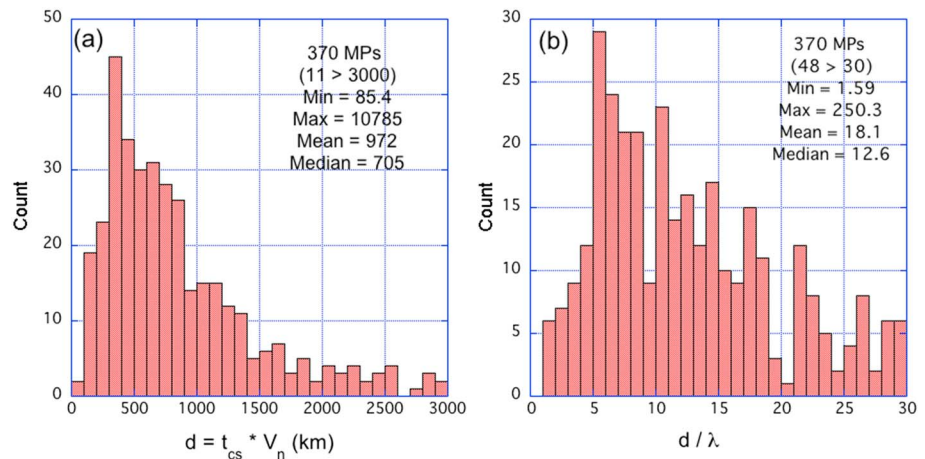


Figure 7. Histograms for (a) d and (b) d/λ_i , based on the $V_{n,mfr}$ for the 370 crossings where $V_{n,mfr}$ and $V_{n,HT}$ agreed within 50% and were consistent with the sign inferred from the sense of the crossings. Requirements were the same as those in Figure 6, plus a de Hoffmann-Teller correlation coefficient >0.90 .

Table 1
Comparison With Earlier Results (Medians for Duration [s], Motion [km/s], and Thickness [km])

	Number	Shear	Duration	Speed	Thickness	Scaled
Berchem and Russell (1982)	30	-	-	≈40	≈800	≈10 ^a
Le and Russell (1994)	22	-	-	≈40	≈400	-
Phan and Paschmann (1996)	128	> 45°	22	34.1	650	13.6 ^a
Haaland et al. (2014)	1,073/583	-	-	48/32	1,396/1,145	13.1/9.9 ^a
Present study	896/370	> 45°	12.9	38.5	705.4	12.6 ^b

^aScaled to the upstream ion gyroradius, r_g . ^bScaled to the upstream ion inertial length, λ_i .

In addition, we also checked the consistency of the sign of the velocities with the sense of the crossings: inbound crossings must have positive normal velocities, outbound, negative velocities. For 370 (= 92.3%) of the 401 crossings, the signs are consistent.

4.3. Thickness

For the 370 crossings, the durations and speeds were multiplied to yield their thicknesses, d , whose distribution is shown in Figure 7a, with a median of 705 km. On the right, Figure 7b shows the same 370 thicknesses, but now scaled to the ion inertial length λ_i , determined from the ion density at the upstream end of the t_{ht} interval. The median scaled thickness is 12.6, and the minimum is 1.6; that is, there are no cases with $d/\lambda_i < 1$.

4.4. Duration, Motion, and Thickness Statistics

Table 1 compares the number of crossings, their durations, speeds, and thicknesses of the present study with those reported earlier. The studies by Berchem and Russell (1982) and Le and Russell (1994) were based on ISEE-1 and ISEE-2 data, using the normal velocities obtained from two-spacecraft timing analysis to turn durations into thicknesses. The Phan and Paschmann (1996) study was based on AMPTE/IRM data, with the thicknesses computed with the bulk velocity in the model LMN coordinates system. The medians for the two ISEE studies in the table were inferred from histograms, and no shear angles were provided. The scaling parameters for the thicknesses in the last two columns were obtained on the upstream, that is, magnetosheath side. Given the differences in methods and crossing numbers, the general agreement between speeds and thicknesses is remarkable, with the exception of the study by Haaland et al. (2014), which is based on Cluster crossings on the flanks of the magnetopause, where the medians were found to be different for the dawn and dusk crossings (shown by the first and second numbers in the table), and absolute thicknesses are substantially larger.

5. Rotational Discontinuity Identification

5.1. Walén Relation

The search for rotational discontinuity (RD) signatures in magnetopause crossings is important, because on the basis of standard MHD models such signatures are associated with ongoing reconnection. In the asymmetric reconnection model by Levy et al. (1964), the magnetosheath side of the magnetopause (away from the reconnection site) consists of an RD, in which the magnetic field direction undergoes a change from its magnetosheath to its magnetospheric orientation and a large increase in plasma velocity occurs, such that the so-called Walén relation holds. When expressed as a jump condition, this relation reads (e.g., Hudson, 1970)

$$\Delta \mathbf{V} = \pm \Delta \mathbf{V}_A \quad (1)$$

where \mathbf{V} is the plasma velocity and \mathbf{V}_A is the Alfvén velocity, corrected for the effect of pressure anisotropy, $\mathbf{V}_A = \mathbf{B}[(1 - \alpha)/\mu_0\rho]^{0.5}$ with $\alpha = (p_{\parallel} - p_{\perp})\mu_0/B^2$. The symbol Δ refers to changes relative to some upstream state. The plus and minus signs apply to situations where the normal magnetic field and velocity components have equal or opposite signs, respectively.

Earthward from the RD is a slow-mode expansion fan, across which the field strength increases and the density decreases. The Walén relation does not hold for this part. The RD and the expansion fan together form the boundaries of a wedge-shaped region on each side of the reconnection site (the X line), in which the rapid, oppositely directed, exhaust jets flow away from the X line. In the symmetric model by Petschek (1964) model, on the other hand, the plasma density and magnetic field strength are the same on the two sides of the magnetopause, while the field direction again changes. Each half of the magnetopause structure then consists

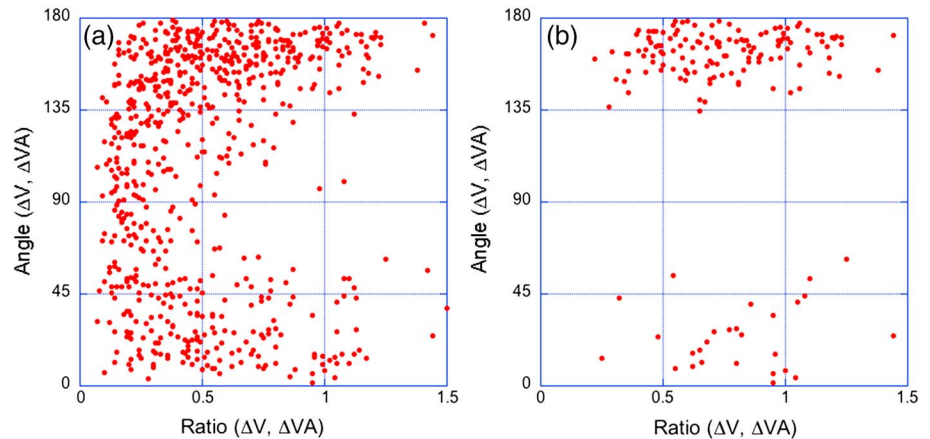


Figure 8. Walén test results. (a) Angle between $\Delta\mathbf{V}$ and $\Delta\mathbf{V}_A$ versus their magnitude ratio, with \mathbf{V}_A corrected for the pressure anisotropy term, for the 731 magnetopause crossings that exclude incomplete and overlapping crossings, and where the velocities at $t_{\max DV}$ are not lower than at the upstream reference time; (b) Same plot but for the 167 events with velocity jumps $\Delta V_l > 250$ km/s and densities at $t_{\max DV} > 1$. In the two plots, 23 and 6 crossings, respectively, have ratios exceeding 1.5 and are thus off scale. Note that the case shown in Figure 1 is the point at an angle of 162° and a ratio of 0.83.

of an RD, immediately followed by a slow shock, the latter at or very near the switch-off limit. The combined RD and switch-off shock again obey the Walén relation for each half of the structure separately, but now with opposite signs in (1), as observed by Sonnerup et al. (2016). The search for RD signatures presented in the paper does not distinguish between the two models, a task left for future work.

The Walén relation can alternatively be formulated as a comparison between the time series of \mathbf{V}' and \mathbf{V}_A (e.g., Paschmann & Sonnerup, 2008, and references therein), where \mathbf{V}' is the velocity evaluated in the de Hoffmann-Teller frame. As pointed out in section 2.2, we do indeed determine the HT velocity and perform the Walén test on the time series, but the time interval, t_{ht} , between the green lines in Figure 1, which we use to determine the HT frame, is usually too long to obtain meaningful results.

Using the jump relation formulation (equation (1)), requires selection of the times between which the jumps in \mathbf{V} and \mathbf{V}_A are to be computed. Following Phan et al. (1996), we have chosen as the upstream reference time the time on the magnetosheath end of the t_{ht} , that is, at the time corresponding to the left green line in the example shown in Figure 1. The end time is taken as the time $t_{\max DV}$, where $|\Delta\mathbf{V}|$ maximizes. By choosing the latter, instead of a time well on the magnetospheric side, we avoid intervals that extend so far earthward that they include measurements in the slow expansion fan in the Levy et al. (1964) model, or worse, measurements from a region of outward plasma flow from the magnetosphere into the magnetosheath, expected in the Petschek (1964) model.

In contrast to Phan et al. (1996), however, we have considered the full 3-D vectors, as in Hudson (1970), rather than only the tangential components, the advantage being that the coordinate system then does not matter for testing the Walén relation.

5.2. Walén Test: All Cases

To present the results of the Walén relation tests in its jump relation form, the most transparent way is to compare the angles between $\Delta\mathbf{V}$ and $\Delta\mathbf{V}_A$, as well as their magnitude ratios, $|\Delta\mathbf{V}/\Delta\mathbf{V}_A|$. Figure 8 shows scatter plots of the angles between $\Delta\mathbf{V}$ and $\Delta\mathbf{V}_A$ versus the magnitude ratios $|\Delta\mathbf{V}/\Delta\mathbf{V}_A|$. Consistent with the expression given below equation (1), the Alfvén velocities have been corrected by the factor $(1 - \alpha)^{0.5}$, which becomes imaginary if $\alpha > 1$, that is, for $p_{\parallel} > p_{\perp}$. Crossings where this occurs have been excluded (see below).

In addition, we have assumed the presence of 4% He^{++} particles by number, close to the average shown in Figure 5b, which reduces the Alfvén velocity by a factor $1/\sqrt{1.16} = 0.928$. Focusing on crossings where the ions are accelerated, we have excluded crossings where the velocity in the exhaust (i.e., at $t_{\max DV}$) is smaller than the velocity at the upstream reference time. That leaves us with 731 crossings, for which results are presented in Figure 8a. Without the $\alpha < 1$ requirement, there would have been 748 cases.

For crossings of an ideal RD, for which there is perfect agreement with equation (1), all points should lie at angles of 0 or 180° and at ratios equal to 1, but in light of the simplifying assumptions that underlie the RD formulas (an ideal MHD current layer that is locally one-dimensional and time stationary), one should not expect perfect agreement. For crossings of the magnetopause when it is not an RD, points could, of course, lie anywhere. As Figure 8a shows, points with ratios less than 0.5 or so occur at all angles, but even above ≈ 0.5 , points are not exactly at 0 or 180°, but form ≈ 30 to 45° wide bands. It is the void in between those bands that supports the conclusion already drawn in earlier publications, that ratios > 0.5 or so can be taken as solid evidence for RD-like crossings (Gosling et al., 1990; Haaland et al., 2014; Paschmann et al., 1986, 2005; Phan et al., 1996, 2013, 2014).

5.3. Walén Test: High-Velocity Cases

With plasma jetting being the primary signature of a reconnecting magnetopause, we next consider only crossings that exhibit large increases in velocity in the outflow region. Taking velocity jumps, $|\Delta\mathbf{V}|$, exceeding 250 km/s, we obtain 266 cases, after excluding two cases with $\alpha > 1$. For typical upstream magnetic fields of 50 nT and densities of 20 cm⁻³, this velocity jump is equal to the Alfvén velocity. Of the 266 crossings, only 125 (47%) meet the RD requirements (here taken as ratios > 0.5 and angular alignment within 30°, in spite of the fact they all had large velocity jumps. In other words, more than half (142) still fail the Walén test.

5.3.1. Cases Failing the Walén Test

Querying the database for the 142 crossings that fail the Walén test, plus visual inspection of plots like the one in Figure 1, reveals that the failed cases fall into essentially three categories (because cases can appear in more than one category, the numbers below, when added exceed 142):

1. In 64 crossings there is some jetting in the north/south (i.e., L) direction, but the angle between $\Delta\mathbf{V}$ and $\Delta\mathbf{V}_A$ is too large and/or their magnitude ratio too far from 1.
2. In 50 crossings, the maximum observed $|\Delta\mathbf{V}|$ is determined by strong flows in the M direction that do not occur at the same time as the maximum in ΔV_L and are not accompanied by commensurate M components of \mathbf{V}_A .
3. In 35 crossings there is essentially no correlation between V and \mathbf{V}_A , but sufficiently large velocities do occur somewhere in the crossing, which the code then picks when searching for the maximum $\Delta\mathbf{V}$.

For the cases in Category 1, it is presently not clear what causes large mismatch, and whether they have anything to do with reconnection at all. Regarding the cases in Category 2, in 24 of them V_M is negatively enhanced on the magnetospheric side. This V_M is thought to be due to the drift of magnetosheath ions penetrating into the magnetosphere and performing partial Larmor orbits, possibly because the MMS spacecraft crossed the reconnection outflow close to the X line (Burch & Phan, 2016; Phan et al., 2016; Shay et al., 2016). The interpretation in terms of flows on the magnetospheric side of the current layer is supported by the fact the plasma density has often already dropped to magnetospheric levels (< 1 cm⁻³), that is, it is much lower than expected in the outflow region. One of the most prominent cases in this set has already been presented in Graham et al. (2017). Finally, the cases in Category 3 are clearly not RDs.

5.3.2. Genuine Jetting Cases

We now consider only those cases that have large velocities along L , the reconnecting field direction, that is, we require large (> 250 km/s) jumps in V_L . In line with the comments in the previous paragraph, we also exclude cases where the density at $t_{\max DV}$ was less than 1 cm⁻³. Figure 8b shows the 167 cases matching these conditions, after excluding one case with $\alpha > 1$. It is now apparent that we essentially lost all the points discussed in the previous section and end up with the cases we consider true RDs, particularly if we relax our RD criterium to ratios above 0.4 and angular agreements within 45°.

5.4. Walén Test: Statistics

Table 2 summarizes our results for the following four event categories:

1. The 731 crossings where the only condition was $|V_{\max}/V_{\text{up}}| \geq 1$. Of these, 30.2% meet the assumed criteria for RDs, that is, ratios between 0.5 and 1.5 and angles $< 30^\circ$ or $> 150^\circ$.
2. The 266 crossings where jetting was defined as $|\Delta\mathbf{V}| \geq 250$ km/s, of which 47% meet the RD criteria, that is, a remarkable 53% fail the test (see section 5.3.1).
3. The 167 crossings where jetting was defined as $|\Delta V_L| \geq 250$ km/s, and the eight cases with densities less than 1 cm⁻³ were excluded, 68.3% meet the RD criteria.

Table 2
Walén Relation Statistics

Ratios and angles	731 crossings ^a	266 crossings ^b	167 crossings ^c	167 crossings ^d
(0.5–1.5) and $\geq 150^\circ$	165	106	97	125
(0.5–1.5) and $\leq 30^\circ$	56	19	17	22
Sums	221 (30.2%)	125 (47.0%)	114 (68.3%)	147 (88.0%)

^aCrossings with $V_{\max}/V_{\text{up}} \geq 1$. ^bAs in footnote a, but $|\Delta\mathbf{V}| \geq 250$ km/s. ^cAs in footnote b, but $|\Delta V_L| \geq 250$ km/s and $N_{\max} \geq 1$. ^dRatios = 0.4–1.6 and angles within 45° .

4. The same 167 crossings, but the RD criteria widened to ratios between 0.4 and 1.6 and angles $\leq 45^\circ$ or $\geq 135^\circ$, which appear reasonable in view of Figure 8b, increasing the percentage to 88.0%.

To put the statistics into context, only about 50 magnetopause crossings had been subjected to Walén relation tests by various authors before 1991, as pointed out by Sonnerup et al. (1995). Then Phan et al. (1996) investigated 69 AMPTE/IRM magnetopause crossings with the same magnetic shear condition as ours ($>45^\circ$), and found that in 61% of the crossings the observed $\Delta\mathbf{V}$ exceeded 50% of $\Delta\mathbf{V}_A$, and when 200 km/s was taken as the lower limit for $|\Delta\mathbf{V}|$, then all but one case met the 0.5 threshold. Why those percentages are higher than ours is not presently understood.

5.5. North-South Asymmetry

Figure 8 shows a strong asymmetry between the number of points at large and small angles (and ratios > 0.5). According to the first and second rows of Table 2, the ratio of the number of points at large and small angles ranges between 5.6 and 5.7 for the cases in columns 3 to 5. We attribute this asymmetry to the dominance of crossings south of the X line in the MMS data, as evidenced by the prevalence of southward directed outflows. South of the reconnection line the normal magnetic field is directed outward (i.e., $B_n > 0$). Together with inward flow ($V_n < 0$), this gives a negative sign in equation (1), that is, oppositely directed $\Delta\mathbf{V}$ and $\Delta\mathbf{V}_A$. The ratio is much smaller (2.9) for the 731 crossings in column 2, because the 731 cases include many crossings of the nonreconnecting or nonlocally reconnecting magnetopause, for which the explanation does not apply. Cases where the X line moved past the spacecraft during the magnetopause crossing so that the jet direction was reversed probably exist in the data set, but our present analysis does not distinguish them from regular magnetopause crossings.

6. Discussion and Conclusions

We have automatically retrieved and analyzed the data from the FGM magnetic field and FPI plasma instruments on MMS1 for 8,670 burst-mode intervals obtained from current sheet crossings near the dayside magnetopause and its environs. Based on a standard set of analyses, we have built a database that can be used to obtain statistics on certain quantities or to select cases with specific properties.

The starting point of the analysis was the identification of the dominant current sheet in each burst-mode interval and the determination of a number of characteristic times within the transition. Magnetic field and plasma quantities on either side of the current sheets and at the other characteristic times are stored. Running standard code on the magnetic field and plasma time series across the current sheets yield additional parameters that bring the total number of quantities stored in the database to 80.

The only manual operation was the classification of the crossings, explained in Appendix A2, which yielded 1,245 sufficiently isolated magnetopause crossings. To characterize the database, we have presented, in section 3, histograms of characteristic properties that help to judge what questions might be addressed with the database.

As the first result, we have presented in section 4 the statistics of the magnetopause current sheet duration, motion, and thickness. The durations span a wide range, from 2.8 to 142 s, with a median of 12.9 s, and the maximum number occurring in the 4-to-6 s bin. Such short durations could not be resolved in the plasma moments from previous missions. Although we only analyzed data from MMS1, we still could, as described in section 4.2, determine the normal magnetopause velocity with two proven single-spacecraft methods, yielding velocities covering a range from 2 km/s to 367 km/s, with a median of 38.5 km/s.

Multiplying crossing durations and velocities, we get magnetopause thicknesses ranging from 85 to 10,800 km, with a median of 705 km. When scaled to the upstream ion inertial length, the thicknesses range between 1.6 and 250. The absence of thicknesses below λ_i would be consistent with the idea that reconnection is more likely to be initiated when or where the current sheet thickness, for one of several possible reasons, has become reduced to the order of λ_i (or r_{gi}), creating an X line at such location(s). Away from any X line or X lines formed in this manner, the current sheet is then widened, as a consequence of the ongoing reconnection. Another possibility is that magnetopause thicknesses less than the ion scale do not occur, regardless of the presence or absence of reconnection, an exception being the electron scale substructure, known to be embedded in the ion-scale diffusion region surrounding an X line during reconnection. Our results indicate that electron scale current sheets that occur on their own, without being embedded in such an ion-scale structure, are not present in the data base.

As shown in Table 1, our medians do not differ much from those reported in previous studies. But given the much larger number of crossings, one can, in possible future studies, easily subdivide the cases according to, for example, local time, solar wind dynamic pressure, upstream β or Mach number, and still have enough samples. Another possible future use is to search for extreme events.

The second result, presented in section 5, concerns the occurrence frequency of rotational discontinuity-like signatures that are used as one of the classical methods to identify ongoing magnetic reconnection. When testing the Walén relation, which characterizes RDs as a jump condition (in section 5.1), one looks at the alignment of the vector jumps in plasma velocity and Alfvén velocity, $\Delta \mathbf{V}$ and $\Delta \mathbf{V}_A$, and at the ratio of their magnitudes.

Figure 8 shows that for ratios above about 0.5, the points lie in two 30 to 45° wide bands, one above 0°, the other below 180°, with a void of points in between. This void is strong evidence that the current sheets with angular alignments within 30 to 45° and magnitude ratios above 0.4 to 0.5 are RD-like structures. Such a wide range might sound overly liberal, but as noted in section 5.2, this range is actually consistent with many earlier studies, but this conclusion was never demonstrated so convincingly as in Figure 8.

The statistics, presented in Table 2, shows that from the 731 magnetopause crossings, about 30% met our RD requirements. For the crossings with $|\Delta \mathbf{V}| > 250$ km/s, the percentage rises to 47%, but a remarkable 53% still fails the test. Reasons for this failure were discussed in detail in section 5.3.1. Replacing the condition $|\Delta \mathbf{V}| > 250$ km/s by $|\Delta V_\perp| > 250$ km/s removes most of the failed cases, as shown in Figure 8b, and 68.3% meet our RD criterium. If we accept even wider ranges for the angles and ratios, as in the last column of Table 2, we would end up with 88% being RDs.

The pronounced asymmetry between the number of points at large and small angles, that is, with negative and positive signs in the Walén relation, can be attributed to the prevalence of MMS crossings south of the reconnection line.

In summary, we have demonstrated that the MMS1 database we have built offers many opportunities for studies not only of the magnetopause but also of other current sheets. It is also important to note that the database is not cast in concrete. It can easily be modified or expanded, for example, by adding more electron data or data from the other MMS spacecraft. Full reprocessing of the entire set of burst-mode intervals on the dayside takes only a day or so on a modern personal computer.

Appendix

A1. Data Retrieval and Ingestion

The first step was to run a script that downloaded the MMS1 data for mission phases 1a and 1b, (20150901–20170209) from the MMS Science Data center, amounting to a total of 8,670 burst-mode intervals. Downloaded measurements include the following:

1. FGM, FPI, and HPCA burst-mode data for the dayside burst-mode intervals (“Events”)
2. FGM survey data for longer (9 min) intervals to provide context
3. OMNI data (IMF, SW; AE, Dst, F107) at 1 min resolution from CDAWeb

The next step was to ingest the data into the QSAS Science Analysis Software (Allen, 2010), where a working list (WL) is created for each “Event.” The WLs are saved, so that postprocessing can be done anytime, while the underlying raw data are deleted to save space. Thereafter, a sequence of analyses on the time series is run,

Plot layout rev. 21 Aug 2017 (3B revised, GSE coords)

20151014_123354

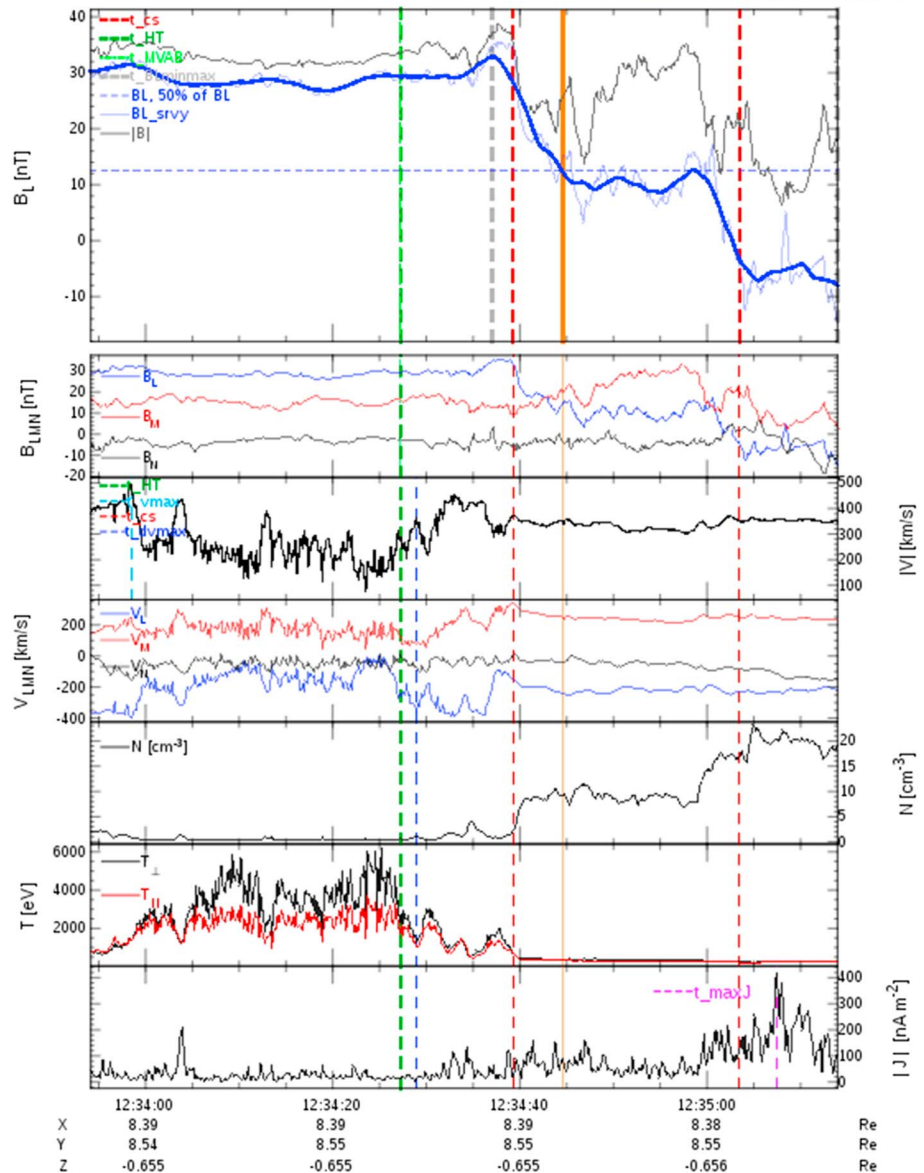


Figure A1. Magnetopause quality: example classified as “monotonic” with “mediocre fit.” Format is the same as the “monotonic,” “good fit” event in Figure 1.

to derive characteristic current sheet parameters for each event. The output from this analysis is then stored in the database, in addition to the data at selected times inside and outside the current layer.

A2. Event Classification

Candidates for magnetopause crossings were obtained by querying the database for events located within $-10R_E < Y_{GSE} < 10R_E$, where the shear across the current sheet is $>45^\circ$ and B_L is >20 nT on what we know would be the magnetospheric side. This yielded 2,446 events, for which the overview plots, like those in Figure 1, were then visually inspected event by event, together with the associated 2 h Quicklook plots, and classified according to the following:

1. the crossing type (magnetopause, magnetosphere, magnetosheath, bow shock, and solar wind)
2. the nature of the B_L profile across the current sheet (“monotonic,” “nonmonotonic”)
3. the quality of the current sheet fit (“good,” “mediocre,” “bad”)
4. the number of current sheets in the burst interval (“single,” “multiple”)

Plot layout rev. 21 Aug 2017 (DB revised, GSE coords)

20151208_080234

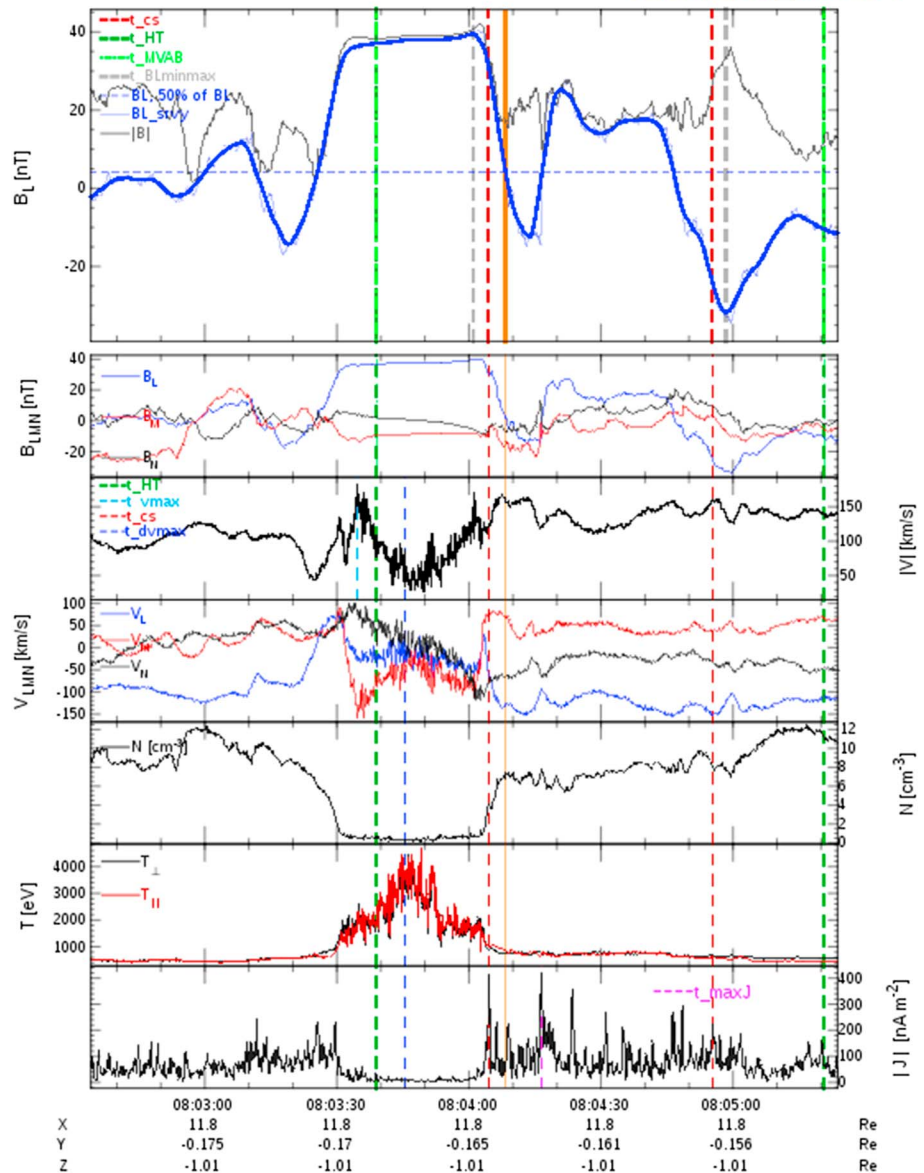


Figure A2. Magnetopause quality: example classified as “nonmonotonic” and “bad fit.”

5. whether the current sheet crossing was “complete,” “incomplete,” or “overlapping” with neighboring current sheets; Harris-like crossings were also noted

The identification of the crossing type is helped by considering asymmetries in plasma density and temperature. The “good,” “mediocre,” and “bad” classification in Item 3 are an eyeball type of assessment of the degree to which the B_L time series resemble a Harris-like profile. Only crossings classified as “complete” were used in this study. This excludes current sheet crossings that were broken up into several burst intervals because we have not concatenated adjacent burst intervals.

Of the 2,446 candidates, only 1,245 were classified as true, sufficiently isolated magnetopause crossings. Most of the remaining ones were found to be magnetosheath current sheets. The five classifications, plus the automatically determined sense of the crossings (inbound versus outbound), are added to the database and can be used for querying. The example in Figure 1 was classified as “magnetopause, monotonic, good fit, single, Harris-like,” while Figure A1 is an example of a “mediocre” fit, and Figure A2 is an example of a “bad” fit, and multiple crossings.

A3. Database Accessibility

If so desired, the database could be made public. It is hosted by the International Space Science Institute in Bern, together with the overview plots for all events (as shown in Figures 1, A1, and A2). The sizes of the database and the plot folder are 18 MB and 760 MB, respectively. QSAS users could also download a folder with the working lists for all events, containing the time series underlying the database, with a total size of 20 GB.

Acknowledgments

MMS data were obtained from the MMS Science Data Center in Boulder at <https://lasp.colorado.edu/mms/sdc/public/> and Solar Wind data from CDAWeb, the Coordinated Data Analysis Web, at <http://cdaweb.gsfc.nasa.gov/about.html>. We thank the many individuals that have served as “Scientists-in-the-Loop” for their careful selection of the burst-mode intervals. Computer code used for the calculations in this paper has been made available as part of the QSAS science analysis system. QSAS is provided by the United Kingdom Cluster Science Centre (Imperial College London and Queen Mary, University of London) supported by the United Kingdom Science and Technology Facilities Council (STFC), freely available at <http://www.sp.ph.ic.ac.uk/csc-web/QSAS/>. G. P. and S. E. H. thank Steve Schwartz and Tony Allen at Imperial College for their continuous support regarding QSAS and are grateful to the International Space Science Institute, Bern, Switzerland, for providing computer resources and infrastructure for data exchange, for hosting the database, and for meeting support. Work at IRAP was performed with support from CNRS and CNES.

References

- Allen, A. J. (2010). QSAS science analysis software. *Astrophysics and Space Science Proceedings*, 11, 225–231. <https://doi.org/10.1007/978-90-481-3499-1-14>
- Berchem, J., & Russell, C. T. (1982). The thickness of the magnetopause current layer—ISEE 1 and 2 observations. *Journal of Geophysical Research*, 87, 2108–2114. <https://doi.org/10.1029/JA087iA04p02108>
- Burch, J. L., & Phan, T. D. (2016). Magnetic reconnection at the dayside magnetopause: Advances with MMS. *Geophysical Research Letters*, 43, 8327–8338. <https://doi.org/10.1002/2016GL069787>
- Burch, J. L., Torbert, R. B., Phan, T. D., Chen, L.-J., Moore, T. E., Ergun, R. E., et al. (2016). Electron-scale measurements of magnetic reconnection in space. *Science*, 352, aaf2939. <https://doi.org/10.1126/science.aaf2939>
- Fuselier, S. A., Lewis, W. S., Schiff, C., Ergun, R., Burch, J. L., Petrinesc, S. M., & Trattner, K. J. (2016). Magnetospheric multiscale science mission profile and operations. *Space Science Reviews*, 199, 77–103. <https://doi.org/10.1007/s11214-014-0087-x>
- Gosling, J. T., Thomsen, M. F., Bame, S. J., Elphic, R. C., & Russell, C. T. (1990). Plasma flow reversals at the dayside magnetopause and the origin of asymmetric polar cap convection. *Journal of Geophysical Research*, 95, 8073–8084. <https://doi.org/10.1029/JA095iA06p08073>
- Graham, D. B., Khotyaintsev, Y. V., Norgren, C., Vaivads, A., André, M., Toledo-Redondo, S., et al. (2017). Lower hybrid waves in the ion diffusion and magnetospheric inflow regions. *Journal of Geophysical Research: Space Physics*, 122, 517–533. <https://doi.org/10.1002/2016JA023572>
- Haaland, S., Sonnerup, B., Dunlop, M., Balogh, A., Georgescu, E., & Hasegawa, H. (2004). Four-spacecraft determination of magnetopause orientation, motion and thickness: Comparison with results from single-spacecraft methods. *Annales Geophysicae*, 22, 1347–1365. <https://doi.org/10.5194/angeo-22-1347-2004>
- Haaland, S., Reistad, J., Tenfjord, P., Gjerloev, J., Maes, L., DeKeyser, J., et al. (2014). Characteristics of the flank magnetopause: Cluster observations. *Journal of Geophysical Research: Space Physics*, 119, 9019–9037. <https://doi.org/10.1002/2014JA020539>
- Harris, E. G. (1962). On a plasma sheath separating regions of oppositely directed magnetic field. *Il Nuovo Cimento*, 23, 115–121. <https://doi.org/10.1007/BF02733547>
- Hudson, P. D. (1970). Discontinuities in an anisotropic plasma and their identification in the solar wind. *Planetary and Space Science*, 18, 1611–1622.
- Khrabrov, A. V., & Sonnerup, B. U. Ö. (1998). Orientation and motion of current layers: Minimization of the Faraday residue. *Geophysical Research Letters*, 25, 2373–2376. <https://doi.org/10.1029/98GL51784>
- King, J. H., & Papitashvili, N. E. (2005). Solar wind spatial scales in and comparisons of hourly Wind and ACE plasma and magnetic field data. *Journal of Geophysical Research*, 110, A02104. <https://doi.org/10.1029/2004JA010649>
- Le, G., & Russell, C. T. (1994). The thickness and structure of high beta magnetopause current layer. *Geophysical Research Letters*, 21, 2451–2454. <https://doi.org/10.1029/94GL02292>
- Levy, R. H., Petschek, H. E., & Siscoe, G. L. (1964). Aerodynamic aspects of the magnetospheric flow. *AIAA Journal*, 2, 2065–2076.
- Paschmann, G., & Sonnerup, B. U. Ö. (2008). Proper frame determination and Walén test. In G. Paschmann, & P. W. Daly (Eds.), *Multi-spacecraft analysis methods, revisited, SR-008 in ISSI Scientific Reports* (Chap. 7, pp. 65–74). Noordwijk, Netherlands: ESA Communications.
- Paschmann, G., Papamastorakis, I., Baumjohann, W., Scokpe, N., Carlson, C. W., Sonnerup, B. U. Ö., & Lühr, H. (1986). The magnetopause for large magnetic shear—AMPTe/IRM observations. *Journal of Geophysical Research*, 91, 11,099–11,115. <https://doi.org/10.1029/JA091iA10p11099>
- Paschmann, G., Haaland, S., Sonnerup, B. U. Ö., Hasegawa, H., Georgescu, E., Klecker, B., et al. (2005). Characteristics of the near-tail dawn magnetopause and boundary layer. *Annales de Geophysique*, 23, 1481–1497.
- Petschek, H. E. (1964). Magnetic field annihilation. In H. Petschek (Ed.), *Proceedings of AAS-NASA symposium on the physics of solar flares* (pp. 425). Washington, DC: NASA.
- Phan, T. D., & Paschmann, G. (1996). Low-latitude dayside magnetopause and boundary layer for high magnetic shear: 1. Structure and motion. *Journal of Geophysical Research*, 101, 7801–7816. <https://doi.org/10.1029/95JA03752>
- Phan, T.-D., Paschmann, G., & Sonnerup, B. U. Ö. (1996). Low-latitude dayside magnetopause and boundary layer for high magnetic shear: 2. Occurrence of magnetic reconnection. *Journal of Geophysical Research*, 101, 7817–7828. <https://doi.org/10.1029/95JA03751>
- Phan, T. D., Shay, M. A., Gosling, J. T., Fujimoto, M., Drake, J. F., Paschmann, G., et al. (2013). Electron bulk heating in magnetic reconnection at Earth's magnetopause: Dependence on the inflow Alfvén speed and magnetic shear. *Geophysical Research Letters*, 40, 4475–4480. <https://doi.org/10.1002/grl.50917>
- Phan, T. D., Drake, J. F., Shay, M. A., Gosling, J. T., Paschmann, G., Eastwood, J. P., et al. (2014). Ion bulk heating in magnetic reconnection exhausts at Earth's magnetopause: Dependence on the inflow Alfvén speed and magnetic shear angle. *Geophysical Research Letters*, 41, 7002–7010. <https://doi.org/10.1002/2014GL061547>
- Phan, T. D., Shay, M. A., Haggerty, C. C., Gosling, J. T., Eastwood, J. P., Fujimoto, M., et al. (2016). Ion Larmor radius effects near a reconnection X line at the magnetopause: THEMIS observations and simulation comparison. *Geophysical Research Letters*, 43, 8844–8852. <https://doi.org/10.1002/2016GL070224>
- Pollock, C., Moore, T., Jacques, A., Burch, J., Gliese, U., Saito, Y., et al. (2016). Fast plasma investigation for magnetospheric multiscale. *Space Science Reviews*, 199, 331–406. <https://doi.org/10.1007/s11214-016-0245-4>
- Russell, C. T., Anderson, B. J., Baumjohann, W., Bromund, K. R., Dearborn, D., Fischer, D., et al. (2016). The magnetospheric multiscale magnetometers. *Space Science Reviews*, 199, 189–256. <https://doi.org/10.1007/s11214-014-0057-3>
- Shay, M. A., Phan, T. D., Haggerty, C. C., Fujimoto, M., Drake, J. F., Malakit, K., et al. (2016). Kinetic signatures of the region surrounding the X line in asymmetric (magnetopause) reconnection. *Geophysical Research Letters*, 43, 4145–4154. <https://doi.org/10.1002/2016GL069034>
- Sonnerup, B., Paschmann, G., Haaland, S., Phan, T., & Eriksson, S. (2016). Reconnection layer bounded by switch-off shocks: Dayside magnetopause crossing by THEMIS D. *Journal of Geophysical Research: Space Physics*, 121, 3310–3332. <https://doi.org/10.1002/2016JA022362>

- Sonnerup, B. U. Ö., & Scheible, M. (1998). Minimum and maximum variance analysis. In G. Paschmann, & P. W. Daly (Eds.), *Analysis methods for multi-spacecraft data, SR-001 in ISSI Scientific Reports* (Chap. 8, pp. 185–220). Noordwijk, Netherlands: Publications Division.
- Sonnerup, B. U. Ö., Paschmann, G., & Phan, T.-D. (1995). Fluid aspects of reconnection at the magnetopause: In situ observations. In B. U. Ö. Sonnerup, G. Paschmann, & T.-D. Phan (Eds.), *Physics of the magnetopause, Geophysical Monograph Series* (Vol. 90, pp. 167). Washington, DC: American Geophysical Union.
- Terasawa, T., Kawano, H., Shinohara, I., Mukai, T., Saito, Y., & Hoshino, M. (1996). On the determination of a moving MHD structure: Minimization of the residue of integrated Faraday's equation. *Journal of Geomagnetism and Geoelectricity*, *48*, 603–614. <https://doi.org/10.5636/jgg.48.603>
- Young, D. T., Burch, J. L., Gomez, R. G., De Los Santos, A., Miller, G. P., Wilson, P., et al. (2016). Hot plasma composition analyzer for the magnetospheric multiscale mission. *Space Science Reviews*, *199*, 407–470. <https://doi.org/10.1007/s11214-014-0119-6>